Catena 135 (2015) 231–239

Contents lists available at ScienceDirect

Catena

journal homepage: www.elsevier.com/locate/catena

Gravity erosion on the steep loess slope: Behavior, trigger and sensitivity

X.-Z. Xu [a,*], Z.-Y. Liu [a], P.-Q. Xiao [b], W.-Z. Guo [a], H.-W. Zhang [c], C. Zhao [a], Q. Yan [a]

[a] School of Hydraulic Engineering, Dalian University of Technology, Dalian 116024, China
[b] Key Laboratory of Process and Control of Soil Loss on the Loess Plateau, Yellow River Institute of Hydraulic Research, Zhengzhou 450003, China
[c] State Key Laboratory of Hydroscience and Engineering, Tsinghua University, Beijing 100084, China

ARTICLE INFO

Article history:
Received 28 February 2015
Received in revised form 7 August 2015
Accepted 11 August 2015
Available online 25 August 2015

Keywords:
Gravity erosion
Laboratory test
Sensitivity analysis
Rainfall
Landform

ABSTRACT

Gravity erosion is a dominant geomorphic process on the widespread steep loess slopes, yet it is not well understood due to the complexity of failure occurrence and behavior. This study conducted a series of experiments in the laboratory to test the stability of different slope geometries and rainfalls and then performed a sensitivity analysis to quantitatively explore the triggering mechanisms of mass failure on the steep loess slope. A topography meter designed by the authors was used to quantitatively measure the process of gravity erosion, and the increase-rate-analysis method presented by the authors was also used to analyze the sensitivity of gravity erosion. The following three types of gravity erosion were observed: landslide, avalanche, and mudslide. In an event of rainfall, various types of gravity erosion might emerge in the same period, and mass failures with the same mode and similar size often adjacently appeared. Sometimes, a group of mass failures might happen on a large, slowly slipping block. Then the increase-rate-analysis method was used to evaluate variations in the gravity erosion with respect to changes in other causal parameters of rainfall duration–intensity and slope height-gradient. Climate-driven factors and topography triggers had prominent influences on gravity erosion. Whether for the total amount or the peak amount in an experiment, the largest sensitivity parameter on both landslides and mudslides was that of rainfall duration. In comparison, topography was relatively less influential. For the total amount in an experiment, the sensitivity parameters of rainfall duration on the landslide and mudslide were 24.9 and 19.5, respectively, while the sensitivity parameter of rainfall intensity on the avalanche was 2.2. For the peak amount in an experiment, the sensitivity parameter of rainfall duration on the landslide and mudslide were 5.5 and 15.6, respectively. Meanwhile the sensitivity parameter of slope gradient on the avalanche was 4.6. The experimental results obtained here provide an insight into the pre-failure mechanisms and processes of steep loess slopes.

1. Introduction

Gravity erosion is a frequent and widespread geomorphological phenomenon, whether in mountainous or urban areas. It is the mass failure on a steep slope, triggered by self-weight. Erosion due to gravitational force occurs under the combined influence of definite hydrologic, geologic, and topographic conditions. Gravity erosion is also an important part of the loss process and is often the first stage in the breakdown and transportation of weathered materials. The phenomena can be classified in part by spatial size and distribution on the ground, or by duration of time that the process acts, or by rate of movement (Shroder and Bishop, 1998; Wang et al., 2014). It may also differ with respect to the thickness of a failed mass, time of failure occurrence, or rotational inclination (Au, 1998). Forms of gravitational erosion include avalanche, landslide, mudflow, and sinkhole formation. Climate and landform play significant roles in the occurrence and behavior of gravity erosion. Gravity erosion generally takes place together with hydraulic erosion, namely, soil loss due to water flowing over the slope, but the mechanism and dynamics of each type of erosion are different. Hence the measures to control hydraulic erosion and gravity erosion are different, and it is essential to quantitatively distinguish the amounts of the failure masses during the same event of rainfall (Xu et al., 2015b).

Most gravity erosion occurs during or just after storms (Ali et al., 2014; Fourie, 1996; Montgomcry and Dietrich, 1994; Peruccacci et al., 2012; Salciarini et al., 2006; Tsai and Yang, 2006). Slope stability problems due to rainfall are often encountered in geotechnical engineering, either in tropic regions with frequent rainfall or in arid regions (Derbyshire et al., 1995; Tsaparas et al., 2002; Tu et al., 2009). Even though an otherwise stable slope may fail due to human-induced factors, such as excavation at the toe or loading due to construction, many slopes simply fail due to rainfall infiltration (Ali et al., 2014; Fourie, 1996). In the area of Three Gorge Reservoir of China, the frequency of rain-induced landslides accounted for 75% of the total geological disasters since building the reservoir (Li et al., 2011). Hence, the determination of geological mechanisms for the occurrence of the rain-induced gravity erosion is a problem of scientific and societal interest.

* Corresponding author.
E-mail address: xzxu@dlut.edu.cn (X.-Z. Xu).

http://dx.doi.org/10.1016/j.catena.2015.08.005
0341-8162/

Assessment of soil erosion sensitivity is defined as the possibility of soil erosion occurrence and identification of areas susceptible to soil erosion when only considering natural factors (Zhang et al., 2013). The main task in landslide susceptibility assessment is to find out how the causal factors influence the occurrence of landslides (Melchiorre et al., 2011). The mode of rain-induced mass failure strongly depends on the initial state of the slope materials, together with the pore water pressure distribution and magnitude of apparent cohesion due to variations in the soil water content (Lourenco et al., 2006; Zhang et al., 2014). Intense rainfall, soils that are largely non-cohesive as they become saturated, steep terrain, and intense development are considered to be the major causes of the failures. Loss of pore-water suction, erosion, and pore-water pressure build-up at shallow depths are the most common ways through which rainwater affects slope stability, as short-burst rainstorms are common. The scale of a failure event depends on the intensity, area, position, and duration of the triggering rainstorm, whereas the antecedent rainfall has relatively little influence (Au, 1998). The erosional history and the consequent morphology are also much more important except for the trimming induced by occasional very large run-off events (Thornes and Alcantara-Ayala´, 1998).

Because gravity erosion is affected and constrained by so many factors, its quantification is complicated and difficult to achieve. Furthermore, gravity erosion is a stochastic, non-continuous process, and usually occurs as a combination of soil transportation with sheet flow and mass failure on the steep slope (Benda and Dunne, 1997; Keefer and Larsen, 2007). Although, the process is readily observed on natural hill slopes, quantifying it in a natural environment is significantly challenging given the extended timeframe between occurrence of the process, and variability in rainfall, soils, and other factors (Acharya et al., 2011). Site-specific and real-time measurement is almost impossible due to the uncertainty and non-continuity of gravity erosion. Hence the volume of individual failure was normally calculated by multiplying the slide area by the thickness of the slide mass after the rainfall events (Guzzetti et al., 2009; Haflidason et al., 2005). Nevertheless, the calculated volume involves an amount of tinkering, for shallow debris flow scars rapidly heal and are difficult to detect after as few as years (Montgomcry and Dietrich, 1994). Moreover, erosion volumes caused by water and gravity could not be distinguished from the above calculation approaches. Landslide activity maps represent a short-cut in the assessment of mass movement hazards (Parise and Wasowski, 1999). While valuable, these inventory maps usually do not provide information on the timing of the events, making it difficult to correlate landslide occurrences with specific triggering events (Kirschbaum et al., 2010).

The specific processes of rain-induced mass failures are most easily studied and quantified in a flume using a rainfall simulator under controlled laboratory conditions (Acharya et al., 2011). Here, we employed a topography meter designed by us to quantitatively measure the process of gravity erosion, and we utilized the increase-rate-analysis method to analyze the sensitivity of gravity erosion. The experimental activity was focused on processes related to gravity and to the interaction between rainfall and topography.

2. Study area

The Loess Plateau is located in the upper and middle reaches of the Yellow River, covering a total area of 624,000 km^2 (Fig. 1). Most of the area is an arid or semi-arid region with dry air, little clouds, and abundant illumination, but is short of moisture. The average annual precipitation on the Loess Plateau is only 350 to 550 mm, most of which is concentrated in the rainy season of June to September (Xu et al., 2004). Usually, a few short yet intense rainfalls can account for more than 60%, even 90%, of the total precipitation in a year.

Areas of the Loess Plateau, especially the Loess Hill Ravine Region and the Loess Mesa Ravine Region, are severely affected by gravity erosion. All types of mass failure are abundant in the area, and locally cover 30–50% of the land (Wang et al., 1993). In the area, rainstorm-induced gravity erosion frequently occurs, because the undulating terrain on the Loess Plateau is characterized by crisscrossing gullies, the vegetation is so sparse, and especially the loess is collapsible and in vertical joints. On the Loess Plateau, a steep bank with the slope more than 70° in the upper reaches of the small watershed is the main source of gravity erosion. Forms of gravity erosion on the Loess Plateau include avalanche, landslide, earth flow, and creep (Tang, 2004).

3. Method and materials

To classify different failure mechanisms and observe conditions of instability, we conducted a series of gully bank collapse experiments under closely controlled conditions in 2010 and 2012 in the Joint Laboratory for Soil Erosion of Dalian University of Technology and Tsinghua University located in Beijing, China. The landscape simulator consisted of a rainfall simulator and a slope model covering an area of 3.0 m by 3.0 m (Fig. 2). Five runs of rainfall were applied in turn on a conceptual landform with a gentle upper slope of 3° and steep lower slope of 70°–80°. An equal period, 12 h or so, was kept after each rainfall to ensure the approximate value of initial water content. The conceptual slope was made with loess by hand patting. The 50% diameter of soil particles, $D50$, was 52.2 μm, and the specific gravity, γ_s, was 2.56. The physical properties of the model soil was similar to that of the Loess Plateau; that is, distribution of the grain size is close that in Shanxi, Gansu, and Shannxi (Xu et al., 2009). A summary of the tests carried out by us is reported in Table 1.

In this experimental study, the failure style was defined by direct eye observation of the process of soil deformation, and the volume of failure mass was calculated according to the video of the topography meter. Both during and 20 min after the rainfall, slope failure occurrence time, slip mode, type of failure scar, location, and slope failure retrogression behavior were recorded by direct observation and the topography meter (Fig. 2). In contrast to the conventional contact observation instruments, the topography meter could quantitatively measure the random mass failures on the steep slope in dynamic environments. The topography meter emitted a group of parallel lasers to the slope surface and recorded the dynamic variation of the steep slope under rainfall simulation with a video camera. Then the operator could transform the plane figures into 3D graphs to compute the shape of the target surface. By comparing the slope geometries in the moments before and after the erosion incident on the snapshot images, we could obtain the soil erosion data, including the volume of any individual slide masses. The instrument was invented by the authors themselves, and its performance was confirmed in the calibration tests and the landslide experiments (Xu et al., 2015a,b).

Gravitational erosion involved both large-scale mass wasting and smaller-scale erosion. The size of each mass failure was calculated and classified, and then the total amount of all failure masses g_t and the peak value of individual erosion events during a rainfall event g_p were obtained. All failure masses with volume more than 500 cm^3 were considered in the experimental study. To assess the effects of the initial landform geometry on the gravity erosion, we divided experiments into the following eight experimental groups, each of which had the same slope height or gradient:

(1) G1 (experiments L5–8) vs G2 (experiments L1–4). Rainfall intensity in the former experimental group was 0.8 mm/min, while the later was 2.0 mm/min.
(2) G3 (experiments L9–10) vs G4 (experiments L5–6). Rainfall duration in the former experimental group was 30 min, while the later was 60 min.
(3) G5 (experiments L1, 3, 5 and 7) vs G6 (experiments L2, 4, 6 and 8). Slope gradient of the initial lower slope in the former experimental group was 70°, while the later was 80°.
(4) G7 (experiments L1, L2, L5 and L6) vs G8 (experiments L3, L4, L7 and L8). Slope height of the initial lower slope in the former experimental group was 1.0 m, while the latter was 1.5 m.

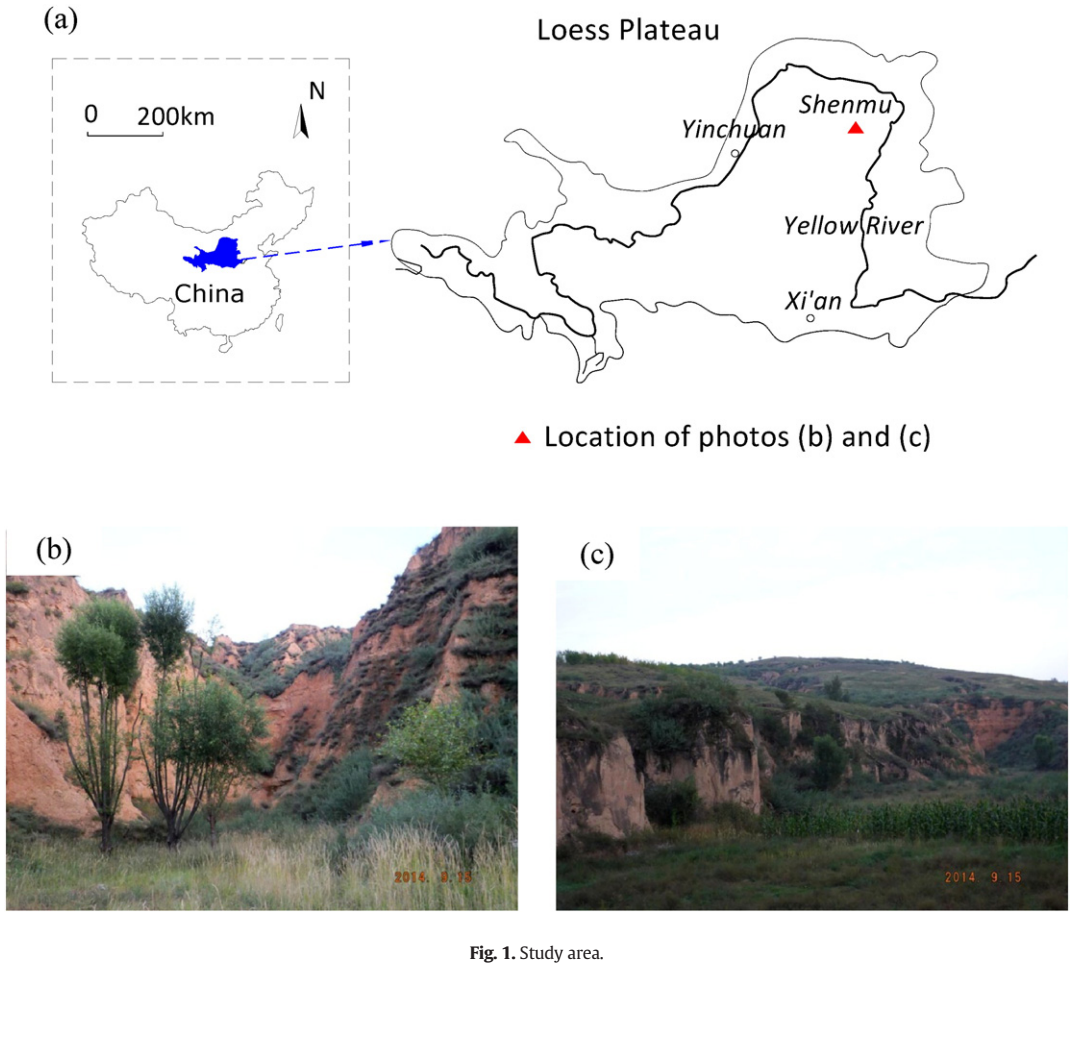

Fig. 1. Study area.

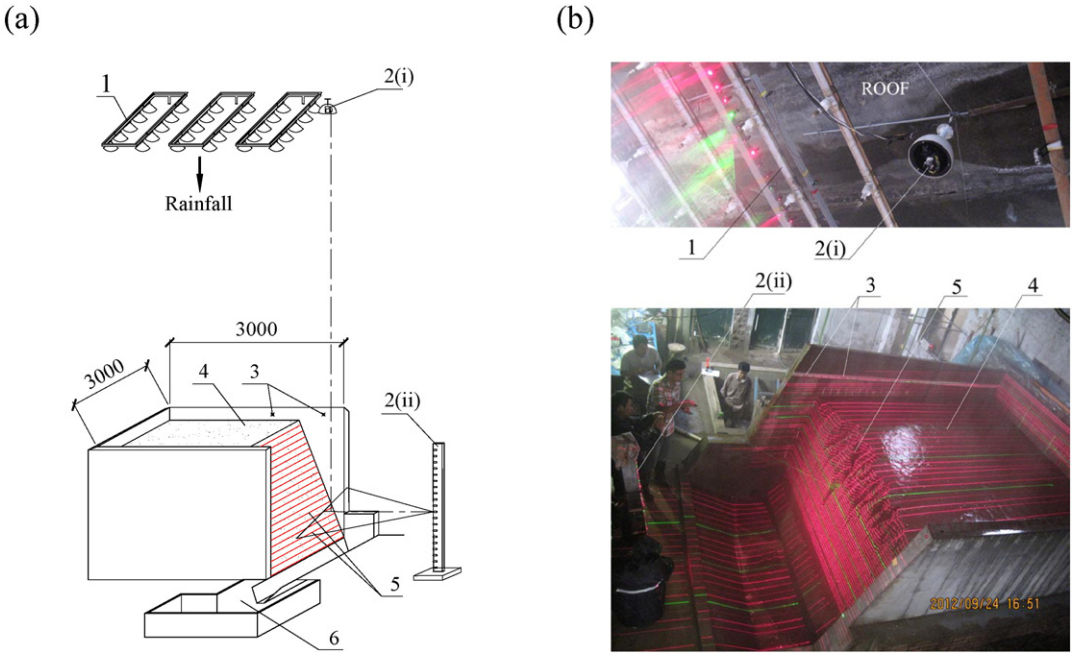

Fig. 2. Landscape simulator in which rainfall simulation experiments were conducted. All units are in millimeters. (a) Blue print of the topography meter measurement system and (b) pictures of the experimental site. 1 rainfall simulator, 2 topography meter (i camera with a collimator and ii laser source), 3 positioning marks, 4 model slope, 5 equidistant horizontal projections, and 6 receiving pool.

Table 1
Testing program.

Test number	Lower slope configuration		Rainfall		
	Height (m)	Gradient (°)	Intensity (mm/min)	Duration (min)	Runs
L1	1.0	70	2.0	30	5
L2	1.0	80	2.0	30	5
L3	1.5	70	2.0	30	5
L4	1.5	80	2.0	30	5
L5	1.0	70	0.8	60	5
L6	1.0	80	0.8	60	5
L7	1.5	70	0.8	60	5
L8	1.5	80	0.8	60	5
L9	1.0	70	0.8	30	5
L10	1.0	80	0.8	30	5

For all groups, the maximum of the individual failure masses and the average value of the total erosion of every experiment were compared. An advantage of the above method is that influences caused by randomness of the gravity could be handily overcome.

Then we used the increase-rate-analysis method to evaluate variations in the gravity erosion with respect to changes in other causal factors such as rainfall intensity and duration, and slope gradient and height. Our sensitivity analysis focuses on g_t and g_p. The increase ratio of gravity erosion R_g (%) is as follows:

$$R_g = (\overline{g}_2 - \overline{g}_1)/\overline{g}_1$$

where $\overline{g}_1$ is the average value of g_t or the maximum value of g_p before the triggering element was changed in an experimental group, cm^3, and $\overline{g}_2$ is that after the triggering element was changed, cm^3. An increased ratio of the above output in percent will be calculated with the growth rate of a parameter while other parameters are fixed in an experimental group:

$$S = R_g/R_t \quad (1)$$

where S is the sensitivity parameter to analyze the sensibility of the failure volume to the triggering elements; $R_t = (t_2 - t_1)/t_1$ is the increased ratio of the triggering element, namely rainfall or landform, in which t_1 is the value before being changed in an experimental group, and t_2 is that after being changed. R_t is conveyed in percent. This approach allows for qualitative investigation of the effect of conditioning factors.

4. Results and discussion

4.1. Occurrence and behavior of the gravity erosion

The failure style is classified such that it reflects the mechanism responsible for failure movement style, failure block moisture, and debris distribution at the location where the movement occurs. All three types of gravity erosion have been observed: landslide, avalanche, and mudslide. A summary of the evolution of slope profiles during events of gravity erosion is given in Figs. 3–5 with reference to the images from the digital video camera. The phenomenon that soil suddenly topples, fragments, and rolls down fully apart from a sloped face is termed avalanche, fall, or collapse; while rock soil on the slope that slips down as a whole along a certain surface of rupture is called landslide. Avalanche is a violent mass failure occurring at steep hillsides. Once released, it may move quite rapidly downhill. The avalanche block is fragmentized, and fully separated from the mother land. Landslide is remarkably characterized with the original properties of the slide block (Li et al., 2011). Generally, the block of landslide integrally moves along the distinct fracture plane—in some cases favored by water, sometimes advancing very quickly, others creeping slowly. Mudslide, i.e., earth flow or mudflow, is defined here as a failure

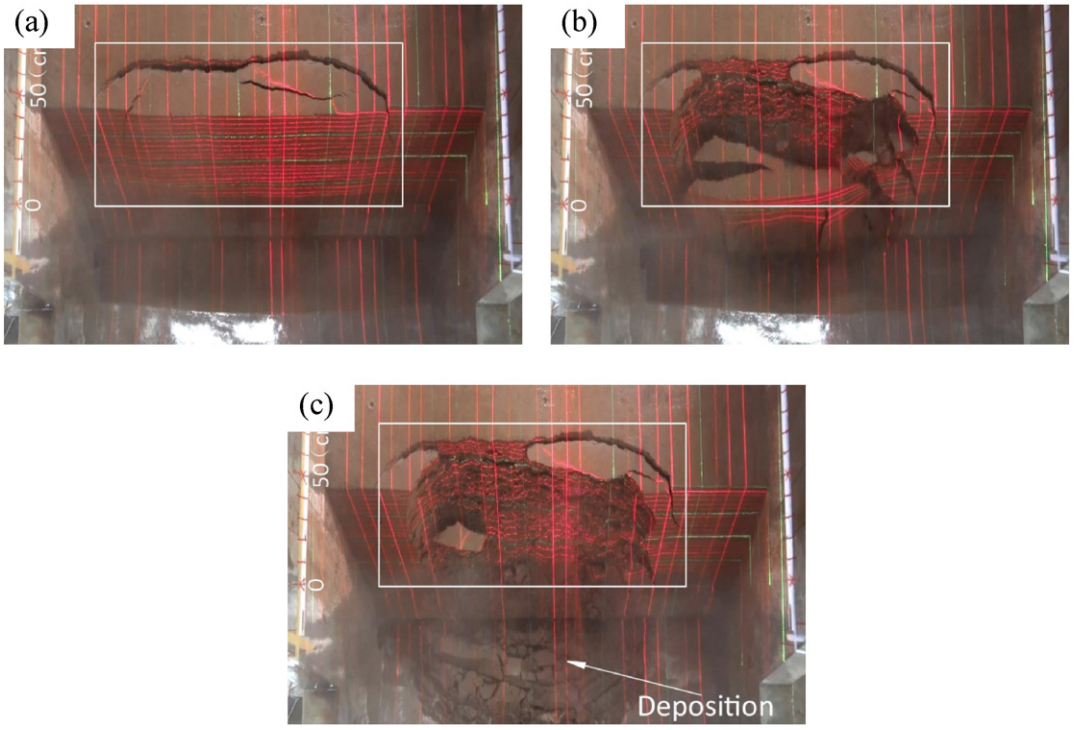

Fig. 3. An avalanche during the first rainfall of test L5. (a) Elapsed time, ET in short, is 58′54″ (58′54″ after the rainfall started). Crevices were creating and expanding which indicated a landslide was coming. (b) ET was 59′01″. The failure block was toppling down, fully separated from the mother land. (c) ET was 59′05″. The failure block was fragmentized and scattered in the gully.

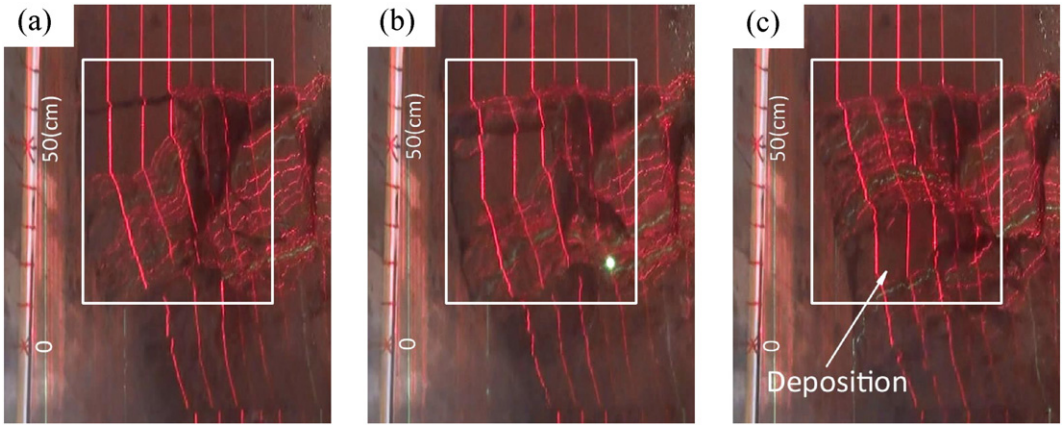

Fig. 4. A landslide during the fourth rainfall of test L6. (a) ET was 37′21″. A landslide started. (b) ET was 37′32″. The landslide block was slipping down as a whole close to the mother land. (c) ET was 37′51″. The landslide block was a one-piece slope body remarkably characterized with the original lithology as the event ended.

occurring with distorted shape of the slope and involving full saturation. It causes full or partial soil liquefaction due to high pore-pressures and may trigger highly mobile soil loss.

In the event of rainfall, various types of gravity erosion may emerge in the same period. Landslide and avalanche grow out of similar geological tectonic environments and lithology structure conditions, and are triggered by the same factors; so landslides in an area are often accompanied by avalanches. On the other hand, mass failures with the same mode and similar size often appear adjacently in the same run of rainfall. For example, 38 min after the start of the second rainfall of experiment L8, a landslide with a volume of 6.75×10^4 cm^3 happened; after 18 min (elapsed time was 56 min), another landslide with the magnitude of 6.3×10^4 cm^3 occurred. Forty-eight minutes after the start of the third rainfall of experiment L8, a landslide with a volume of 4.16×10^4 cm^3 happened; 11 min later (elapsed time was 59 min), another landslide with the magnitude of 3.83×10^4 cm^3 occurred.

Some mass movement processes act very slowly, while others occur suddenly. In the present laboratory experiments, an interesting phenomenon, termed *compound landslide*, was observed: a group of mass failures including avalanche, mudslide, or landslide might happen on a large, slowly slipping block. The process could last for several minutes, or more than 10 min during a 1 hour rainfall event. To distinguish the compound landslide from other individual gravity erosion events has practical significance. When we calculate the total amount of gravity erosion in a rainfall event, we could calculate the volume of the compound landslide with the screenshots in the moments before and after the longstanding landslide and need not care about the incidents that happened on the sliding block. Surely, deviation that resulted from the hydraulic erosion still existed, but the error was so small compared to the large landslide that it could be ignored. Fig. 6 shows an event of compound mass failure on the steep loess slope in the fourth rainfall of test L5. When a large block was sliding, two avalanches in relatively small bulk happened on the block. Because the avalanches occurred on the slip mass during the compound landslide, the erosion volume of the compound landslide was the difference of the slope volume in the white frame between Fig. 6a and f.

4.2. Triggers: rainfall intensity and duration

Changes in rainfall and terrain severely influence sediment dynamics, e.g., erosion and retention processes (Ali et al., 2014; Sánchez-Canales et al., 2015). The erosional history and the consequent morphology are also much more important than the trimming induced by occasional very large run-off events (Thornes and Alcantara-Ayala´, 1998). For any experiment with the same initial landform, the total volume of the mass failures after five rainfalls, which might be transported to the lower reaches by the gully flow, illustrated the potential contribution of gravity erosion to the soil loss from the catchment. On the other hand, the maximum volume of the individual failure masses indicated possible harm on the local building construction or to human lives. For all groups, the average value of total erosion and the maximum of individual failure masses of every experiment are listed in Tables 2 and 3. Here, WGE, Whole Gravity Erosion, means the sum of avalanche, landslide, and mudslide.

Rainwater infiltrating to soil might decrease the anti-shearing strength of the failure surface, and consequently induce gravity erosion on the steep slope (Li et al., 2011). Rainfall intensity and duration are the most immediate impact factors on gravity erosion. Inspection of Fig. 7 reveals that the total volume of avalanche was enlarged by 111% and the maximum volume of individual avalanche was augmented by 65% if the rainfall intensity was increased from 0.8 to 2.0 mm/min, namely: a 150% increase in rainfall intensity. At the same time, the amounts of

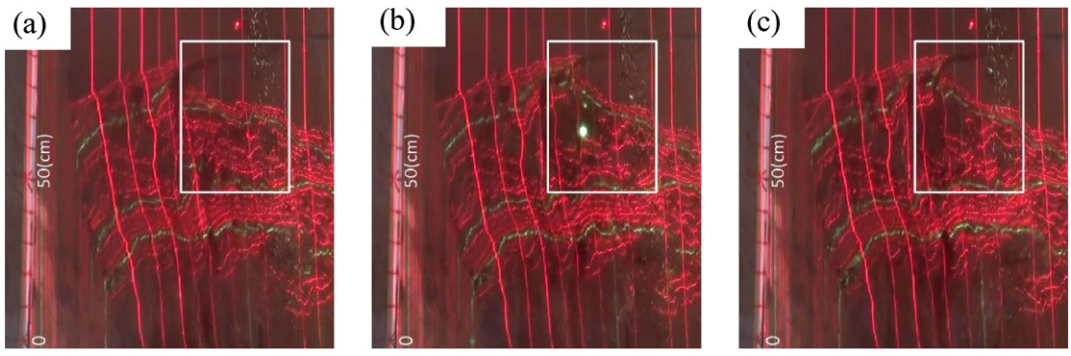

Fig. 5. A mudslide during the fourth rainfall of test L6. (a) ET was 58′55″. Landform before a mudslide. (b) ET was 59′18″. A mudflow was initiated at the top-left corner of the white frame. (c) ET was 59′48″. The mud flow with high water content was in close proximity to liquid form.

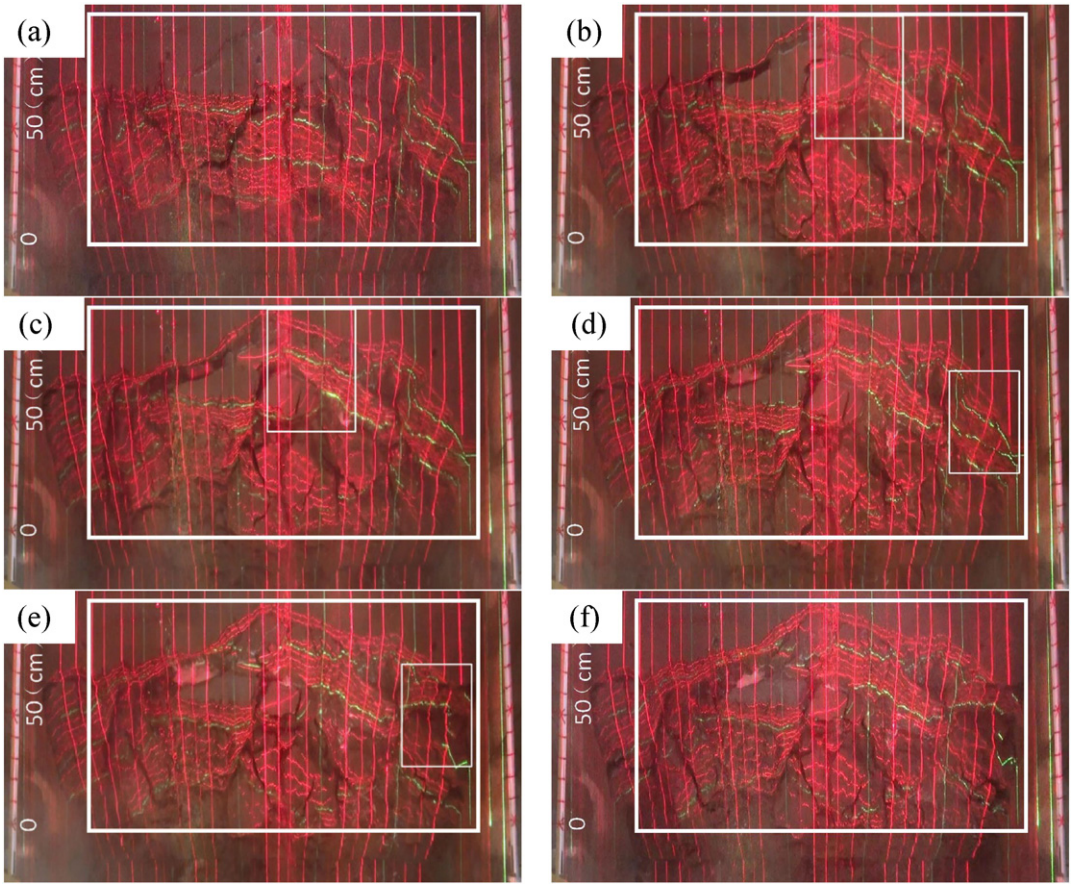

Fig. 6. An event of compound mass failure during the fourth rainfall of test L5. Because the avalanches occurred on the slip mass in the period of the compound landslide, the erosion volume of the compound landslide was the difference of the slope volume in the white frame between a and f. (a) ET was 39′26″. This is the terrain before a compound landslide. (b) ET was 40′32″ and (d) ET was 41′09″. Landforms in the small white frame rectangles are those before avalanches happened. (c) ET was 40′50″ and (e) ET was 41′43″. Landforms in the small white frame rectangles are those after avalanches happened. (f) ET was 42′11″. Here is the failure scar caused by the compound landslide.

landslide and mudslide were only a little reduced. Hence rainstorm with high intensity and a long period could give rise to avalanches with relatively larger range and bulk.

Fig. 8 portrays increments of the mass failure as the rainfall duration increased. If the rainfall intensity was kept constant at a low intensity, 0.8 mm/min, while the duration increased from 30 to 60 min—namely, a 100% increase in rainfall duration—the volume of avalanche was not relatively obviously enlarged, but total volumes of the landslide and mudslide were augmented to 24.9 and 19.5 times, and the maximum volumes of individual landslide and mudslide were augmented 5.5 and 15.6 times, respectively. In conclusion, the loess slope under light rain is more easily subjected to landslide and mudflow as rainfall increases in duration.

In the experiments, a clear relation has been found between the failure style and the rainfall mode, i.e., intensity or duration. Nevertheless, the result is so different from that in other geographic regions described by Lourenco et al. (2006), where no clear relation was found between the pore water pressure and the failure mode.

4.3. Triggers: slope height and gradient

Topography is another significant factor associated with soil erosion. An increase of slope gradient will result in enlarged gravity erosion. The scatter diagram in Fig. 9 shows increments of the mass failure as the slope gradient was increased. When other conditions were fixed but the slope gradient increased from 70° to 80°—i.e. a 14% increase in slope gradient—the total amount of landslide was increased by 52%,

Table 2
Total volumes of different failure types for an initial landform after five rainfalls. High-magnitude failure events with the erosion amount more than 500 cm^3 were analyzed.

Experimental group	Average of a type of initial landform (10^3 cm^3/m)			
	Avalanche	Landslide	Mudslide	WGE
G1 (L5–L8)	97.1	98.7	4.8	200.6
G2 (L1–L4)	204.6	66.4	3.0	274.0
G3 (L9–L10)	52.4	4.7	0.4	57.5
G4 (L5–L6)	66.1	122.6	7.3	196.0
G5 (L1, L3, L5, L7)	142.7	65.4	6.1	214.3
G6 (L2, L4, L6, L8)	159.0	99.7	1.7	260.3
G7 (L1, L2, L5, L6)	136.0	112.5	4.1	252.6
G8 (L3, L4, L7, L8)	165.7	52.6	3.6	222.0

WGE, namely the whole gravity erosion, means a sum of avalanche, landslide and mudslide.

Table 3
The maximum volume of a type of mass failure for an initial landform after five rainfalls. High-magnitude failure events with the erosion amount more than 500 cm^3 were analyzed.

Experimental group	Peak of the individual failure events (10^3 cm^3)			
	Avalanche	Landslide	Mudslide	WGE
G1 (L5–L8)	224.1	177.6	21.7	224.1
G2 (L1–L4)	369.9	168.4	24.6	369.9
G3 (L9–L10)	75.2	27.1	1.3	75.2
G4 (L5–L6)	60.7	177.6	21.7	177.6
G5 (L1, L3, L5, L7)	224.1	177.6	24.6	224.1
G6 (L2, L4, L6, L8)	369.9	168.4	7.2	369.9
G7 (L1, L2, L5, L6)	139.5	177.6	24.6	177.6
G8 (L3, L4, L7, L8)	369.9	156.0	12.8	369.9

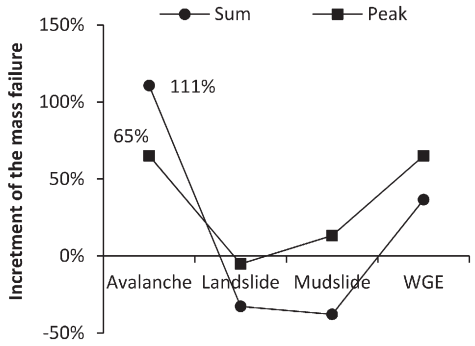

Fig. 7. Increment of the mass failure as the rainfall intensity was increased by 150%.

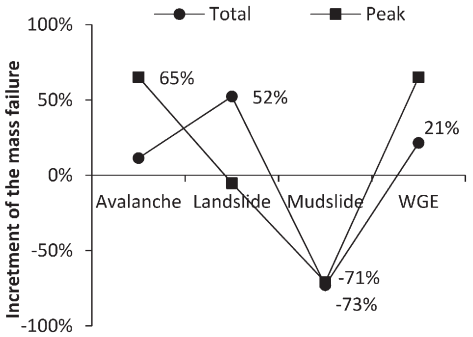

Fig. 9. Increment of the mass failure as the slope gradient was increased by 14%.

and the maximum amount of individual avalanche was increased by 65%. Nevertheless, both the total and maximum amounts of the mudslide were decreased by more than 70%. In fact, as the slope gradient grew, the total amount of WGE was increased by 21%, by virtue of the relatively large erosion bulks of the avalanche and landslide.

Slope height also has an important influence on gravity erosion. Avalanche is a high-speed movement of the soil mass torn instantly from its parent. The potential energy of a collapsed mass, which depends on its volume and height, has a direct impact on the erosion amount. While other conditions were fixed but the slope height increased from 1.0 to 1.5 m—i.e. a 50% increase in slope height—the total amount of avalanche was increased by 22%, and the maximum volume of individual avalanche was augmented by 165%, as shown in Fig. 10. In contrast, landslide and mudflow are soil slides drawn by gravity along the slope. Their potential energies are weakened by the friction of slope, so that the influence of the slope height is relatively small. To our surprise in the experiments, a small decrease occurred on the amounts of landslide and mudslide when the slope height increased from 1.0 to 1.5 m. The reason may be the randomness of the gravity erosion or the deviation of the experiment.

4.4. Causes of different failures: a concise discussion

Factors that induce gravity erosion include the following two main categories (Liu et al., 2013; Wu and Sidle, 1995): (1) internal factors that have decisive effects on landslides, i.e. geology, geomorphology, soil property, vegetation cover, flow distribution and fractures, and (2) external factors that trigger landslides suddenly, such as rainfall, earthquake and flood. Mass failures are common in the Loess Plateau due to the presence of macro pores, well-developed vertical jointing, and susceptibility to water infiltration (Zhang and Liu, 2010; Zhang et al., 2009). Loess has typical landforms like vertical joints and loose textures, as well as special physical and mechanical properties, such as low water content, strong structural strength, and weaker water resistance (Li et al., 2013). Most mass failures are triggered by slope cutting and heavy rainfall (Zhuang and Peng, 2014). Enhanced by human activities, precipitation infiltrates into the interior of the loess formations along structural joints and openings caused by weathering (Zhang et al., 2015). Steep-cut slopes encourage the concentration of shear stress at the foot of the slope and tension stress at the top, leading to the formation of cracks in the inner slope, and followed by slope failure.

It could be seen that on the sides of the platforms, ridges and domes are the steep slopes which could easily slide in favor to soil failure, such as infiltration of rain water, irrigation water, and earthquake effects. Generally, loess landslides occur on slopes steeper than 35° and higher than 40 m, and the sliding is more likely to occur on concaves slopes (Li et al., 2013). An investigation on the Loess Plateau by Cao (1981) illustrates that landslides generally happened on a slope with a gradient of 35°–55°, and most of the avalanches occurred on scarps steeper than 55°. Landslides were common in the middle and lower reaches of the gully, whereas avalanches were frequent on the banks of the gully or of the river, especially on the gully head. Investigations in the northern Shaanxi Province (Li et al., 2013) shows that 80% of loess landslides occurred in slopes with dip angles exceeding 35°, and failure style was normally collapse-sliding or purely collapsed as the slope angle became greater than 50°. On the other hand, increments of different failures due to landform and rainfall have been described in Sections 4.2 and 4.3 of this paper.

4.5. Sensitivity analysis

Sensitivity analyses were conducted to evaluate the conditions required for the initiation of storm-induced gravity erosion. Our analysis identified the parameters related to the natural environment as the most influential for failure occurrence and behavior. The results are summarized in Fig. 11a and b. It is clear that with the increase of factors of rainfall duration–intensity and slope height-gradient, in most cases both the total and peak amount of gravity erosion during a rainfall event were enlarged. For the total amount in an experiment, the sensitivity parameters of rainfall duration on the landslide, mudslide, and WGE were 24.9, 19.5, and 2.4, respectively, and the sensitivity parameter of rainfall intensity on the avalanche was 2.2. For the peak amount in

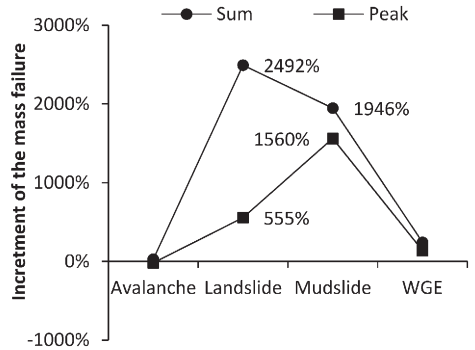

Fig. 8. Increment of the mass failures as the rainfall duration was increased by 100%.

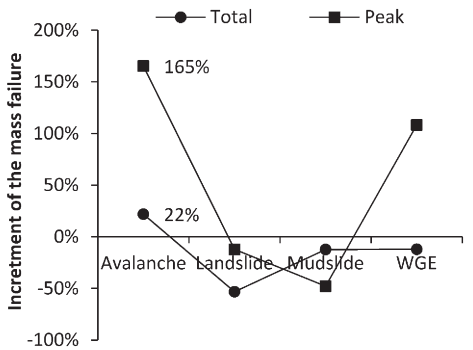

Fig. 10. Increment of the mass failure as the slope height was increased by 50%.

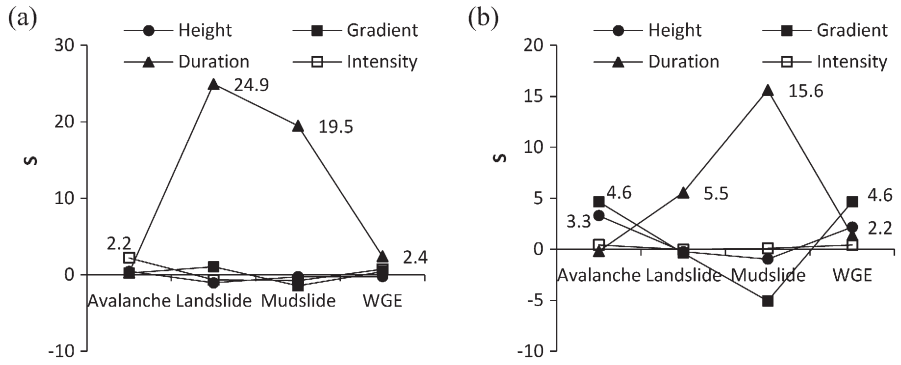

Fig. 11. Sensitivity analysis of the triggers. (a) Total amount and (b) Peak of the individual event.

an experiment, the sensitivity parameters of rainfall duration on the landslide and mudslide were 5.5 and 15.6, respectively. Meanwhile the sensitivity parameters of the slope gradient on the avalanche and WGE were both 4.6. All of the parameters mentioned above were much larger than those of other triggers listed in the Fig. 11a and b. It is worth mentioning that slope height was the second most influential element on the maximum gravity erosion, of which sensitivity parameters on the peak values of avalanche and WGE were 3.3 and 2.2, respectively. Nevertheless, the majority of the sensitivity parameters shown in Fig. 11 are less than or close to 1.0, which is much smaller than the maximum values above mentioned.

Accordingly, small changes in variables such as the duration and intensity of rainfall events could cause major changes in gravity erosion, demonstrating the significant sensitivity of these dynamics to climate change on the Loess Plateau. The result also suggests that rainfall duration–intensity and slope height-gradient are the prominent influential inputs on the steep loess slope. It is worth noting that both of these factors are potentially climate-driven: rainfall directly and landform through the effects of temperature and moisture on the soil's organic content (Sánchez-Canales et al., 2015). Collectively, a positive increment of those variables is associated with a positive increment of the failure amount and thus of the susceptibility level. If we compare the degree of vertical variability of the variable relief with the variable rainfall, we can observe that the strength of influence of the relief is lower than the rainfall.

For the sensitivity analysis, an increase-rate-analysis method was tested, which has never been previously employed in landslide susceptibility studies. As explained earlier, the aim of sensitivity analysis was to detect trends, interactions between variables, and non-linear behaviors. The approach allows a deeper understanding of the failure mechanism, especially when we want to recognize the effect of each causal factor and of the combination of factors on the susceptibility to gravity erosion. The method is easy to understand, facile to calculate, and its result is easy to read. It holds promise for research in other relevant fields of soil and water conservation.

4.6. Problems and suggestions

This study will provide a tool for more reliable identification and analysis of site conditions associated with different types of failure. It is important, however, to note that although flume experiments are possibly the best approach to simulate natural slope failures, extrapolating these results to natural conditions requires caution because natural soil variability and initial stress conditions are difficult to reproduce in a flume study (Lourenco et al., 2006). Presently field tests on gravity erosion have been conducted by the authors in the Liudaogou Catchment of the Loess Plateau, and a comparison between the laboratory and field studies will be reported in the near future. The method of sensitivity analysis presented here is a novel way to evaluate the role of erosion triggers, especially in processing the results with limited data in the experimental study. However, reliability of the analysis conclusions depends on the original data obtained in the laboratory or field. An in-depth qualitative review of the erosion rule will give great help to the test design and sensitivity analysis.

Vegetation also appeared to play a distinct role in controlling the locations of landslides at this site (Shakoor and Smithmyer, 2005). In the vegetated areas, plant roots acted as a binder adding to soil strength, and thus reinforcing soils and improving their stability on slopes (Easson and Yarbrough, 2002; Shields and Gray, 1993; Waldron and Dakessian, 1981). Thus experiments on the landform with different vegetation covers are expected in the future. Finally, mechanical properties of soil, such as cohesion, friction angle, and density play an immediate role in the interpretation of mass failure behavior. Thus, a sensitivity analysis was also worth performing to evaluate variations in the factor of safety with respect to changes in the above mechanical parameters.

5. Conclusions

The experimental results obtained here provide insights into the pre-failure mechanisms and erosion processes of steep loess slopes. In an event of rainfall, various types of gravity erosion might emerge in the same period, and mass failures with the same mode and similar size often appeared adjacently in the same run of rainfall. *Compound landslide*, a group of mass failures might happening on a large slowly slipping block, was also observed in the tests.

Climate-driven factors and topography triggers had prominent influences on gravity erosion. Whether for the total amount or the peak amount in an experiment, the largest sensitivity parameter on both the landslide and mudslide was that of rainfall duration. In comparison, topography was relatively less influential. The sensitivity parameter of the slope gradient was the highest influence on the avalanche for the peak of an individual event.

Acknowledgments

This study is supported in part by the National Natural Science Foundation of China (51179021; 51039003; 51079016) and the Open Research Fund Program of Key Laboratory of Process and Control of Soil Loss on the Loess Plateau (2014001). The first author wishes to sincerely thank Professor Guang-Qian Wang for his encouraging and constructive advice. The first author also wishes to acknowledge the three anonymous referees for their very positive and useful suggestions.

References

Acharya, G., Cochrane, T., Davies, T., Bowman, E., 2011. Quantifying and modeling post-failure sediment yields from laboratory-scale soil erosion and shallow landslide experiments with silty loess. Geomorphology 129, 49–58.

Ali, A., Huang, J., Lyamin, A.V., Sloan, S.W., Cassidy, M.J., 2014. Boundary effects of rainfall-induced landslides. Comput. Geotech. 61, 341–354.
Au, S.W.C., 1998. Rain-induced slope instability in Hong Kong. Eng. Geol. 51, 1–36.
Benda, L., Dunne, T., 1997. Stochastic forcing of sediment supply to channel networks from landsliding and debris flow. Water Resour. Res. 33, 2849–2863.
Cao, Y.Z., 1981. Mechanism and prediction of the gravity erosion on the loess area. Bull. Soil Water Conserv. 4, 19–23 (in Chinese).
Derbyshire, E., Asch, T.V., Billard, A., Meng, X., 1995. Modelling the erosional susceptibility of landslide catchments in thick loess: Chinese variations on a theme by Jan de Ploey. Catena 25, 315–331.
Easson, G., Yarbrough, L.D., 2002. The effects of riparian vegetation on bank stability. Environ. Eng. Geosci. 8, 247–260.
Fourie, A.B., 1996. Predicting rainfall-induced slope instability. Proc. Inst. Civ. Eng. Geotech. Eng. 119, 211–218.
Guzzetti, F., Ardizzone, F., Cardinali, M., Rossi, M., Valigi, D., 2009. Landslide volumes and landslide mobilization rates in Umbria, central Italy. Earth Planet. Sci. Lett. 279, 222–229.
Haflidason, H., Lien, R., Sejrup, H.P., Forsberg, C.F., Bryn, P., 2005. The dating and morphometry of the Storrega Slide. Mar. Pet. Geol. 22, 187–194.
Keefer, D.K., Larsen, M.C., 2007. Assessing landslide hazards. Science 316, 1136–1137.
Kirschbaum, D.B., Adler, R., Hong, Y., Hill, S., Lerner-Lam, A., 2010. A global landslide catalog for hazard applications: method, results, and limitations. Nat. Hazards 52, 561–575.
Li, H.Z., Yang, Z.S., Wang, T.R., Pan, Y.Z., 2011. Recognition of Landslide and Case Studies. Wuhan University of Technology Press, Wuhan, pp. 19–43 (in Chinese).
Li, T., Wang, C., Li, P., 2013. Loess deposit and loess landslides on the Chinese Loess Plateau. In: Shan, W., Fathani, T.F. (Eds.), Progress of Geo-Disaster Mitigation Technology in Asia. Springer Berlin Heidelberg, pp. 235–261.
Liu, C., Li, W., Wu, H., Lu, P., Sang, K., Sun, W., Chen, W., Hong, Y., Li, R., 2013. Susceptibility evaluation and mapping of China's landslides based on multi-source data. Nat. Hazards 69, 1477–1495.
Lourenco, S.D.N., Sassa, K., Fukuoka, H., 2006. Failure process and hydrologic response of a two layer physical model: implications for rainfall-induced landslides. Geomorphology 73, 115–130.
Melchiorre, C., Castellanos Abella, E.A., van Westen, C.J., Matteucci, M., 2011. Evaluation of prediction capability, robustness, and sensitivity in non-linear landslide susceptibility models. Guanta 'namo, Cuba. Comput. Geosci. UK 37, 410–425.
Montgomcry, D.R., Dietrich, W.E., 1994. A physically based model for the topographic control on shallow landsliding. Water Resour. Res. 30, 1153–1171.
Parise, M., Wasowski, J., 1999. Landslide activity maps for landslide hazard evaluation: three case studies from Southern Italy. Nat. Hazards 20, 159–183.
Peruccacci, S., Brunetti, M.T., Luciani, S., Vennari, C., Guzzetti, F., 2012. Lithological and seasonal control on rainfall thresholds for the possible initiation of landslides in central Italy. Geomorphology 139–140, 79–90.
Salciarini, D., Godt, J.W., Savage, W., Conversini, P., 2006. Modeling regional initiation of rainfall-induced shallow landslides in the eastern Umbria Region of central Italy. Landslides 3, 181–194.
Sánchez-Canales, M., López-Benito, A., Acuña, V., Ziv, G., Hamel, P., Chaplin-Kramer, R., Elorza, F.J., 2015. Sensitivity analysis of a sediment dynamics model applied in a Mediterranean river basin: global change and management implications. Sci. Total Environ. 502, 602–610.
Shakoor, A., Smithmyer, A.J., 2005. An analysis of storm-induced landslides in colluvial soils overlying mudrock sequences, southeastern Ohio, USA. Eng. Geol. 78, 257–274.
Shields, F.D., Gray, D.H., 1993. Effects of woody vegetation on the structural integrity of sandy levees. JAWRA 28, 917–931.
Shroder, J.F., Bishop, M.P., 1998. Mass movement in the Himalaya: new insights and research directions. Geomorphology 26, 13–35.
Tang, K.L., 2004. Soil and Water Conservation in China. Science Press, Beijing, pp. 100–104 (in Chinese).
Thornes, J.B., Alcantara-Ayala', I., 1998. Modelling mass failure in a Mediterranean mountain environment: climatic, geological, topographical and erosional controls. Geomorphology 24, 87–100.
Tsai, T.L., Yang, J.C., 2006. Modeling of rainfall-triggered shallow landslide. Environ. Geol. 50, 525–534.
Tsaparas, I., Rahardjo, H., Toll, D.G., Leong, E.C., 2002. Controlling parameters for rainfall-induced landslides. Comput. Geotech. 29, 1–27.
Tu, X.B., Kwong, A.K.L., Dai, F.C., Tham, L.G., Min, H., 2009. Field monitoring of rainfall infiltration in a loess slope and analysis of failure mechanism of rainfall-induced landslides. Eng. Geol. 105, 134–150.
Waldron, L.J., Dakessian, S., 1981. Soil reinforcement by roots: calculation of increased soil shear resistance from root properties. Soil Sci. 132, 427–435.
Wang, D.F., Zhao, X.Y., Ma, H.L., Yao, B.S., 1993. An investigation on the gravity erosion on the loess area. Soil Water Conserv. China 12, 26–28 (in Chinese).
Wang, F., Zhang, C., Peng, Y., Zhou, H., 2014. Diurnal temperature range variation and its causes in a semiarid region from 1957 to 2006. Int. J. Climatol. 34, 343–354.
Wu, W., Sidle, R.C., 1995. A distributed slope stability model for steep forested watersheds. Water Resour. Res. 31, 2097–2211.
Xu, X., Zhang, H., Zhang, O., 2004. Development of check-dam systems in gullies on the Loess Plateau, China. Environ. Sci. Pol. 7, 79–86.
Xu, X.-Z., Liu, Z.-Y., Wang, W.-L., Zhang, H.-W., Yan, Q., Zhao, C., Guo, W.Z., 2015a. Which is more hazardous: avalanche, landslide, or mudslide? Nat. Hazards 76, 1939–1945.
Xu, X.-Z., Zhang, H.-W., Xu, S.-G., Wang, W.-L., 2009. Effects of dam construction sequences on soil conservation efficiency of a check-dam system. J. Beijing For. Univ. 31, 1392–2144 (in Chinese).
Xu, X.Z., Zhang, H.W., Wang, W.L., Zhao, C., Yan, Q., 2015b. Quantitative monitoring of gravity erosion using a novel 3D surface measuring technique validation and case study. Nat. Hazards 75, 1927–1939.
Zhang, A., Zhang, C., Chu, J., Fu, G., 2015. Human-induced runoff change in Northeast China. J. Hydrol. Eng. 20, 04014069.
Zhang, C., Wang, D., Wang, G., Yang, W., Liu, X., 2014. Regional differences in hydrological response to canopy interception schemes in a land surface model. Hydrol. Process. 28, 2499–2508.
Zhang, D., Wang, G., Luo, C., Chen, J., Zhou, Y., 2009. A rapid loess flowslide triggered by irrigation in China. Landslides 6, 55–60.
Zhang, M.S., Liu, J., 2010. Controlling factors of loess landslides in western China. Environ. Earth Sci. 59, 1671–1680.
Zhang, R., Liu, X., Heathman, G.C., Yao, X., Hu, X., Zhang, G., 2013. Assessment of soil erosion sensitivity and analysis of sensitivity factors in the Tongbai–Dabie mountainous area of China. Catena 101, 92–98.
Zhuang, J., Peng, J., 2014. A coupled slope cutting—a prolonged rainfall-induced loess landslide: a 17 October 2011 case study. Bull. Eng. Geol. Environ. 73, 997–1011.